Supporting information

MYCELIAL EFFECTS ON PHAGE RETENTION DURING TRANSPORT IN A MICROFLUIDIC PLATFORM

Nawras Ghanem[1], Claire E. Stanley[2], Hauke Harms[1,3], Antonis Chatzinotas[1,3] and Lukas Y. Wick[1*]

[1]*Helmholtz Centre for Environmental Research - UFZ, Department of Environmental Microbiology, Permoserstraße 15, 04318 Leipzig, Germany.*

[2]*Agroecology and Environment Research Division, Agroscope, Reckenholzstrasse 191, 8046 Zurich, Switzerland*

[3]*German Centre for Integrative Biodiversity Research (iDiv) Halle-Jena-Leipzig, Deutscher Platz 5e, 04103 Leipzig, Germany*

Number of pages: 14

Number of figures: 2

Number of tables: 2

[*] Corresponding author: Mailing address: Helmholtz Centre for Environmental Research - UFZ. Department of Environmental Microbiology; Permoserstrasse 15; 04318 Leipzig, Germany. phone: +49 341 235 1316, fax: +49 341 235 45 1316, e-mail: lukas.wick@ufz.de.

MICROFLUIDIC DEVICE DESIGN AND PREPARATION

Microfluidic devices were prepared as described in Stanley et al.[1] In brief: A polyester film photolithography mask (Micro Lithography Services Ltd., UK) and a 100 mm silicon wafer (Silicon Materials, Germany), spin-coated with a 10 µm thick layer of SU-8 photoresist (MicroChem, USA), were used to create the master mold. The channel architecture was based on the fluid exchange device, detailed in Stanley et al.,[2] and enables active pumping of solutions into the observation chamber (Fig. 1). Two versions of the design were made, one that allows a mycelium to occupy the observation chamber and one that does not (Fig. S3). The latter design enables control measurements to be performed (i.e., in the absence of a mycelium). Polydimethylsiloxane (PDMS) silicone elastomer was then prepared and poured onto the master mold. PDMS was prepared using a 10:1 ratio of base to curing agent (Sylgard 184, Dow Corning, USA) that was mixed thoroughly and degassed prior to pouring. After curing overnight at 70 °C, the PDMS was removed from the mold and diced into slabs. A precision cutter (Syneo, USA), having a cutting edge diameter of 1.02 mm, was used to punch the holes for the medium inlet and outlet as illustrated in Fig. 1 and Fig. S3. The PDMS slabs were washed in 0.5 M sodium hydroxide, 70 % v/v ethanol, and sterile double distilled water (ddH2O) and then dried at 70 °C for 1 h. They were then bonded to glass-bottomed Petri dishes (World Precision Instruments) and sterilized for 20 minutes under ultraviolet light.

Fluorinated ethylene polymer (FEP) tubing (inner diameter: 0.80 mm, outer diameter: 1.60 mm; Cole-Parmer, Germany), hollow steel pin connectors (20 ga; Instech Laboratories, USA) and connector pins fitted with a luer-lock adaptor (20 ga; Instech Laboratories, USA) were used to connect the syringe to the microfluidic device and subsequently allow a variety of test solutions to be introduced into the observation channel (in the presence or absence of a mycelium). Fig. 1 shows an overview of the microfluidic setup for clarity.

MICROFLUIDIC DEVICE: CHARACTERIZATION OF FLOW CONDITIONS

The microfluidic device (channel height: 10 µm; channel width: 1000 µm; channel length: 6 mm) operates at laminar flow conditions (i.e. is a laminar flow reactor) with a Reynold's number (Re) equal to ca. 0.003 (eq. S1).

$$Re = \frac{QD_H}{vA} = \frac{1.4 \times 10^{-12}\, m^3/s \times 2 \times 10^{-5} m}{1 \times 10^{-6} m^2/s \times 1 \times 10^{-8} m^2} = \frac{2.8 \times 10^{-17} m^4/s}{1.0 \times 10^{-14} m^4/s} = 0.003 \quad \text{(S1)}$$

where:

Q = volumetric flow rate (m^3/s); i.e.: Q = 5 µL h^{-1} = 5 × 10^{-6} L h^{-1} = 1.4 × 10^{-12} (m^3 s^{-1})

D_H = hydraulic diameter (m), $D_H = \frac{4 \times \text{cross sectional area}}{\text{wetted perimeter}} = \frac{4 \times 10000\ \mu m^2}{2020\ \ \mu m} = 20\ \mu m = 2 \times 10^{-5} m$

V = kinematic viscosity (m^2/s); i.e. 1.0 × 10^{-6} m^2/s (for water)

A = cross sectional area (m^2); i.e. 10,000 µm^2 = 1.0 × 10^{-8} m^2

A syringe pump ensured that the volumetric flow rate in the microchannels is controlled by adjusting the pressure needed to produce the required flow rate independent of channel geometry.[3] As the microchannels within this microfluidic device have a rectangular profile (with a high width: height ratio, i.e. 1000/10 = 100), the velocity distribution profile across the microchannel is highly uniform.[4]

Hence, taking the average velocity of the system to be 1.4×10^{-4} m s^{-1} (average velocity = volumetric flow rate / cross section area), we estimate that it would take ca. 43 seconds for the fluid to reach the outflow (i.e. to traverse the entire observation chamber) assuming a channel length of 6×10^{-3} m.

CALCULATION OF THE XDLVO INTERACTION ENERGIES OF PHAGE DEPOSITION

The phage-mycelia interaction energy ($G_{\mathrm{XDLVO}}(h)$) at a distance h (nm) between two surfaces was calculated using the extended DLVO (XDLVO) theory (cf. eq. S2) based on the sphere-plate model.[5] The XDLVO theory thereby is an extension of the DLVO approach, which is the sum of G_{EDL}, G_{LW} and the Born repulsion energy G_{Born}. In the XDLVO theory, the energy $G_{\mathrm{XDLVO}}(h)$ is composed of the electrostatic repulsion (G_{EDL}), the Lifshitz-van der Waals (G_{LW})[6] and the acid−base (G_{AB}) interaction energy (eq. S2).[5]

$$G_{\mathrm{XDLVO}}(h) = G_{\mathrm{AB}} + G_{\mathrm{EDL}}(h) + G_{\mathrm{LW}}(h) \quad \text{(S2)}$$

The DLVO approach does not consider the polar forces that are supposed to be dominant forces between particles in polar media.[7] Additionally, the acid-base (G_{AB}) interaction energy was reported in many studies to be essential in explaining the interaction behavior between approached particles.[5,8]

Acid-base interaction energy (G_{AB})

Eq. S3 was applied to calculate the acid-base interaction energy (G_{AB}):[9,5]

$$G_{AB}(h) = 2\pi a_P \Delta G^{AB} \lambda \exp\left(\frac{l_0 - h}{\lambda}\right) \quad \text{(S3)}$$

Where a_P is the radius of phages, and h is the separation distance between the phage and the mycelial surface. The λ is the characteristic decay length of AB interaction in water (estimated to be 0.6 nm).[10] The acid-base interaction energy depends on the Gibbs free energy of the phage and the fungus as given by eq. S3. ΔG^{AB} is the acid-base component of the free energy interaction at contact given by eq. S4:[10,7]

$$\Delta G^{AB} = [2\left(\sqrt{\gamma_P^+} - \sqrt{\gamma_F^+}\right)\left(\sqrt{\gamma_P^-} - \sqrt{\gamma_F^-}\right) - \left(\sqrt{\gamma_P^+} - \sqrt{\gamma_l^+}\right)\left(\sqrt{\gamma_P^-} - \sqrt{\gamma_l^-}\right) - \left(\sqrt{\gamma_F^+} - \sqrt{\gamma_l^+}\right)\left(\sqrt{\gamma_F^-} - \sqrt{\gamma_l^-}\right)] \quad \text{(S4)}$$

The surface Gibbs free energy of phage γ_P and the fungal γ_F surfaces (mJ m^{-2}) were calculated based on the measured contact angles (θ) of phages, membrane filters and fungal surfaces using water, formamide and methylene iodide as liquids by applying the Young equation according to eq. S5:

$$cos(\theta) = -1 + 2\frac{\sqrt{\gamma_P^{LW}\gamma_l^{LW}}}{\gamma_l^{total}} + 2\frac{\sqrt{\gamma_P^{+}\gamma_l^{-}}}{\gamma_l^{total}} + 2\frac{\sqrt{\gamma_P^{-}\gamma_l^{+}}}{\gamma_l^{total}} \quad \text{(S5)}$$

The total surface Gibbs free energy (γ^{total}) is separated in a Lifshitz-van der Waals (γ^{LW}) and an acid-base component (γ^{AB}) and is represented by eq. S6. The electron acceptor and the electron donor components of acid-base surface energy γ^+ and γ^- is shown in eq. S7.

$$\gamma^{total} = \gamma^{AB} + \gamma^{LW} \quad \text{(S6)}$$

$$\gamma_i^{AB} = 2\sqrt{\gamma_i^{+}\gamma_i^{-}} \quad \text{(S7)}$$

Following van Oss et al.[11] we calculated the phage parameters γ_p, γ_p^{LW}, γ_p^{+}, γ_p^{-}, while literature data was utilized for water, formamide and methyleneiodide.[12]

Electrostatic repulsion energy (G_{EDL})

Eq. S8 was applied to calculate the electrostatic repulsion energy between phages and the fungal surface:[13]

$$G_{EDL} = \pi\varepsilon_0\varepsilon_r a_p\{2\zeta_p\zeta_F \ln\left[\frac{1+\exp(-\kappa h)}{1-\exp(-\kappa h)}\right] + (\zeta_p^2 + \zeta_F^2)\ln[1-\exp(-2\kappa h)] \quad \text{(S8)}$$

where κ^{-1} is the thickness of the electrical double layer (EDL, nm) as calculated by the Guoy-Chapman theory with C and z being the molar bulk concentration and the charge number of the electrolytes, respectively (eq. S9).

$$\kappa^{-1} = [3.29zC^{1/2}]^{-1} \quad \text{(S9)}$$

For a 100 mM buffer solution a κ^{-1} of 0.65 nm was calculated.[12]

Lifshitz-van der Waals interaction energy (G_{LW})

Using the values of the effective Hamaker constant (eq. S11), the Lifshitz-van der Waals interaction energy can be approximated by eq. S10:[7,12]

$$G_{LW} = -\frac{A_{132}}{6}\left[\frac{2a_p(h+a_p)}{h(h+a_p)} - \ln\left(\frac{h+2a_p}{h}\right)\right] \quad \text{(S10)}$$

The Hamaker constant A_{132} is described by eq. S11:[14]

$$A_{123} = (\sqrt{A_{11}} - \sqrt{A_{33}})(\sqrt{A_{22}} - \sqrt{A_{33}}) \quad \text{(S11)}$$

Here, A_{ii} denotes the individual Hamaker constant for phages (A_{11}), hyphae (A_{22},) and water (A_{33}). A_{33} was taken from the literature,[14] while A_{11} and A_{22} were calculated by eq. S12.

$$A_{ii} = 6\pi l_0^{\,2} \gamma_i^{LW} \quad \text{(S12)}$$

According to Fowkes,[15] the value of $6\pi l_0^2$ equals 1.44×10^{-18} m^2, with l_0 being the equilibrium separation distance between the phage and the fungus (0.157 nm).[11]

Table S1. Overview of the surface Gibbs free energy (γ) and the contact angles of water (θ_w), formamide (θ_f) and methylene iodide (θ_m) for the phages and hyphae studied.

Name	Contact angle (Θ)			Surface free energy (mJ m^{-2})[1]				
	Θ_w	Θ_f	Θ_m	γ^-	γ^+	γ^{AB}	γ^{LW}	γ^{Tot}
water	-	-	-	25.5*	25.50*	51.0*	21.8*	72.8*
formamide	-	-	-	39.6*	2.30*	19.0*	39.0*	58.0*
methylene iodide	-	-	-	< 0.1*	< 0.1*	≈ 0*	50.8*	50.8*
membrane filter Anodisc 25	23	-	-	-	-	-	-	-
T4	95	61	40	0.1	0.30	0.2	39.5	39.7
PSA-HS2	40	31	43	34.6	0.96	11.5	38.0	49.5
Pythium ultimum	62	47	72	17.3	4.49	17.6	21.8	39.4
Coprinopsis cinerea	131	106	131	0.0	4.47	0.2	1.5	1.7

* Surface free energy data for water, formamide and methylene iodide taken from.[12]

Table S2. Composition of the YMG and CCMM media use for *C. cinerea*.[1]

Medium	**Composition**
Yeast-malt extract-glucose (YMG) medium	0.4 % w/v yeast extract, 1 % w/v malt extract, 0.4 % w/v glucose, 1.5 % w/v agar
C. cinerea minimal medium (CCMM)	5 g L^{-1} glucose, 2 g L^{-1} asparagine, 50 mg L^{-1} adenine sulfate, 1 g L^{-1} KH_2PO_4 , 2.25 g L^{-1} Na_2HPO_4, 0.29 g L^{-1} Na_2SO_4, 0.5 g L^{-1} 2di-ammonium tartrate, 0.04 mg L^{-1} thiamine hydrochloride, 0.25 g L^{-1} $MgSO_4$, 5 mg L^{-1} *p*-aminobenzoic acid (pABA).

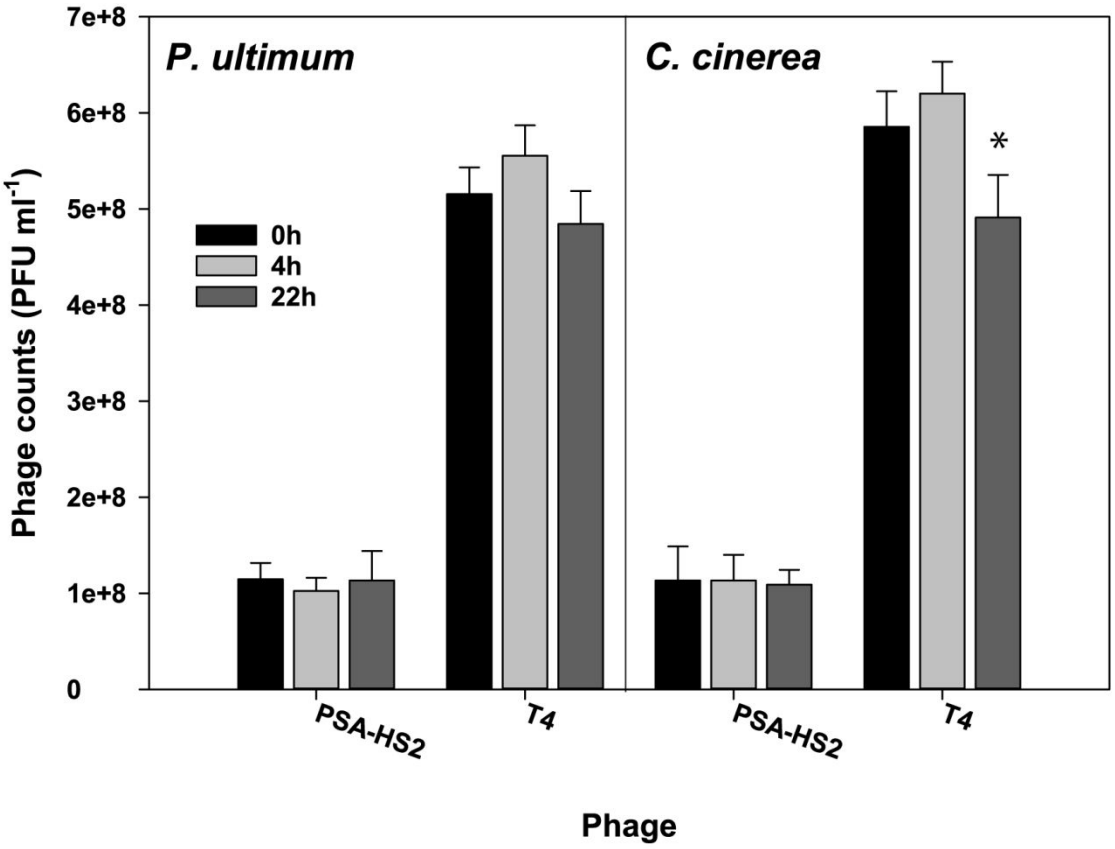

Figure S1. Stability and viability of the PSA-HS2 and T4 phage suspensions after exposure to *P. ultimum* and *C. cinerea* conditioned media (at $t = 0$, 4 and 22 h). The results represent the average and standard deviations of triplicate experiments using phage quantification by PFU. T4 counts in the presence of *C. cinerea* conditioned medium at $t = 22$ h were statistically different to initial concentrations at $t = 0$ and $t = 4$ h, as indicated by the asterisk ($p \leq 0.05$).

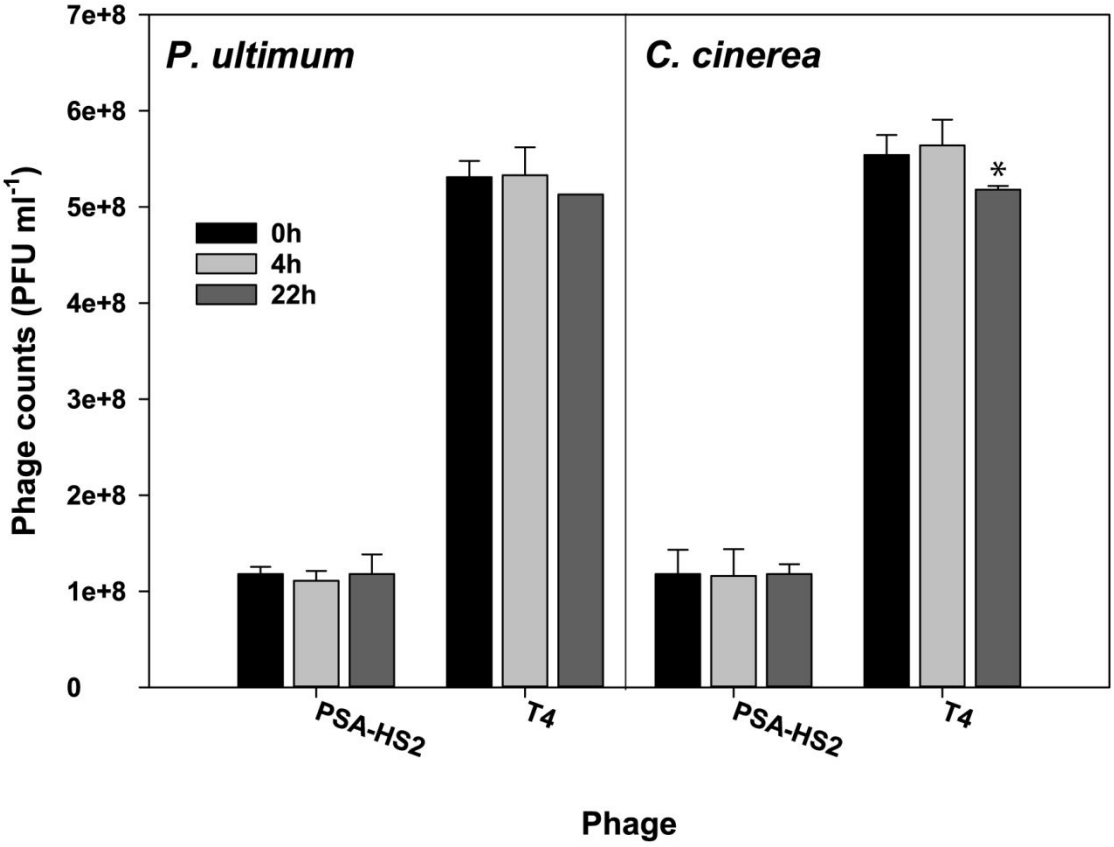

Figure S2. Stability and viability of the PSA-HS2 and T4 phage suspensions after exposure to fresh media i.e. LB and CCMM media for *P. ultimum* and *C. cinerea,* respectively at $t = 0$, 4 and 22 h. The results represent the average and standard deviations of triplicate experiments using phage quantification by PFU. T4 counts in the presence of *C. cinerea* conditioned medium at $t = 22$ h were statistically different to initial concentrations at $t = 0$ and $t = 4$ h, as indicated by the asterisk ($p \leq 0.05$).

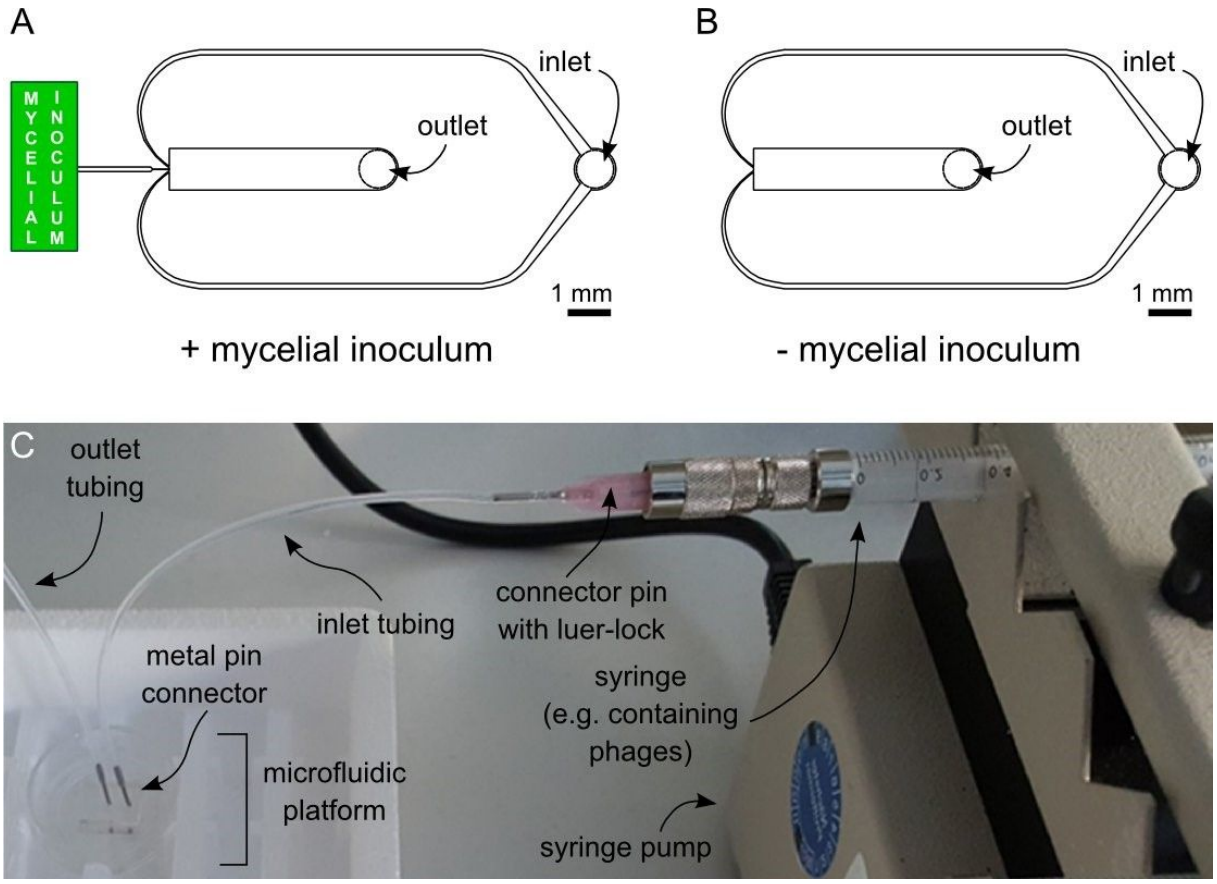

Figure S3. Design and operation of the experimental setup. (A) Two-dimensional representation of the microfluidic platform with a mycelial inoculum that was placed next to the lateral opening of the microfluidic device, allowing hyphae to penetrate and grow into the observation channel via a constriction channel. (B) Two-dimensional representation of the microfluidic platform that enables control measurements to be performed (i.e. in the absence of a mycelium). (C) Photograph illustrating the experimental setup, where a syringe pump was used to drive phage suspensions into the microfluidic channels in the presence and absence of mycelia.

REFERENCES

(1) Stanley, C. E.; Stöckli, M.; Swaay, D. van; Sabotič, J.; Kallio, P. T.; Künzler, M.; deMello, A. J.; Aebi, M. Probing Bacterial–fungal Interactions at the Single Cell Level. *Integr. Biol.* **2014**, *6* (10), 935–945. https://doi.org/10.1039/C4IB00154K.

(2) Stanley, C.; Shrivastava, J.; Brugman, R.; Heinzelmann, E.; Frajs, V.; Bühler, A.; van Swaay, D.; Grossmann, G. Fabrication and Use of the Dual-Flow-RootChip for the Imaging of Arabidopsis Roots in Asymmetric Microenvironments. *BIO-PROTOCOL* **2018**, *8* (18). https://doi.org/10.21769/BioProtoc.3010.

(3) Mavrogiannis, N.; Ibo, M.; Fu, X.; Crivellari, F.; Gagnon, Z. Microfluidics Made Easy: A Robust Low-Cost Constant Pressure Flow Controller for Engineers and Cell Biologists. *Biomicrofluidics* **2016**, *10* (3). https://doi.org/10.1063/1.4950753.

(4) Stone, H. A. Introduction to Fluid Dynamics for Microfluidic Flows. In *CMOS Biotechnology*; Lee, H., Westervelt, R. M., Ham, D., Eds.; Series on Integrated Circuits and Systems; Springer US: Boston, MA, 2007; pp 5–30. https://doi.org/10.1007/978-0-387-68913-5_2.

(5) Chrysikopoulos, C. V.; Syngouna, V. I. Attachment of Bacteriophages MS2 and _X174 onto Kaolinite and Montmorillonite: Extended-DLVO Interactions. *Colloids and Surfaces B: Biointerfaces* **2012**, *92*, 74–83. https://doi.org/10.1016/j.colsurfb.2011.11.028.

(6) Hermansson, M. The DLVO Theory in Microbial Adhesion. *Colloids and Surfaces B: Biointerfaces* **1999**, *14* (1), 105–119.

(7) Van Oss, C. J.; Giese, R. F.; Costanzo, P. M. DLVO and Non-DLVO Interactions in Hectorite. *Clays Clay Miner* **1990**, *38* (2), 151–159.

(8) Attinti, R.; Wei, J.; Kniel, K.; Sims, J. T.; Jin, Y. Virus' (MS2, ΦX174, and Aichi) Attachment on Sand Measured by Atomic Force Microscopy and Their Transport through Sand Columns. *Environmental Science & Technology* **2010**, *44* (7), 2426–2432. https://doi.org/10.1021/es903221p.

(9) Tadros, T. Interfacial Forces in Aqueous Media, Carel J. van Oss, Marcel Dekker Inc., New York, 1994. *J. Chem. Technol. Biotechnol.* **1995**, *64* (3), 311–311. https://doi.org/10.1002/jctb.280640321.

(10) van Oss, C. J.; Docoslis, A.; Wu, W.; Giese, R. F. Influence of Macroscopic and Microscopic Interactions on Kinetic Rate Constants: I. Role of the Extended DLVO Theory in Determining the Kinetic Adsorption Constant of Proteins in Aqueous Media, Using von Smoluchowski's Approach. *Colloids and Surfaces B: Biointerfaces* **1999**, *14* (1–4), 99–104. https://doi.org/10.1016/S0927-7765(99)00028-4.

(11) Van Oss, C. J.; Chaudhury, M. K.; Good, R. J. Interfacial Lifshitz-van Der Waals and Polar Interactions in Macroscopic Systems. *Chemical Reviews* **1988**, *88* (6), 927–941.

(12) Sharma, P. K.; Hanumantha Rao, K. Adhesion of Paenibacillus Polymyxa on Chalcopyrite and Pyrite: Surface Thermodynamics and Extended DLVO Theory. *Colloids and Surfaces B: Biointerfaces* **2003**, *29* (1), 21–38. https://doi.org/10.1016/S0927-7765(02)00180-7.

(13) Boks, N. P.; Norde, W.; van der Mei, H. C.; Busscher, H. J. Forces Involved in Bacterial Adhesion to Hydrophilic and Hydrophobic Surfaces. *Microbiology* **2008**, *154* (10), 3122–3133. https://doi.org/10.1099/mic.0.2008/018622-0.

(14) Van Oss, C. J.; Good, R. J.; Chaudhury, M. K. The Role of van Der Waals Forces and Hydrogen Bonds in "Hydrophobic Interactions" between Biopolymers and Low Energy Surfaces. *Journal of Colloid and Interface Science* **1986**, *111* (2), 378–390. https://doi.org/10.1016/0021-9797(86)90041-X.

(15) Fowkes, F. M. Attractive Forces at Interfaces. *Industrial & Engineering Chemistry* **1964**, *56* (12), 40–52.